

Collisional redistribution and saturation of near-resonance scattered light*

J. L. Carlsten, A. Szöke,[†] and M. G. Raymer[‡]

Joint Institute for Laboratory Astrophysics, University of Colorado and National Bureau of Standards, Boulder, Colorado 80309

(Received 9 September 1976)

This paper reports on our studies of near-resonant scattering of laser light in a collisional environment. A pulsed dye laser with a peak power of 55 MW/cm² was tuned near the 460.73-nm resonance line of strontium and the side emission was observed from an oven containing both strontium vapor and argon buffer gas. The emission was composed of three spectral components: Rayleigh scattering at the frequency of the laser ω_L , fluorescence at the resonance frequency ω_0 of strontium, and a third component at $2\omega_L - \omega_0$. These three components have been studied as a function of the frequency and intensity of the laser and also as a function of the argon buffer gas pressure. While the Rayleigh emission was found to vary as Δ^{-2} ($\Delta = \omega_0 - \omega_L$), the fluorescence component, which was produced by Sr-Ar collisions, was found to be asymmetric with the sign of Δ as predicted by line-broadening theory. By measuring the ratio of the intensities of the fluorescence and Rayleigh components, we were able to measure directly the collisional redistribution function, important in the study of radiative transfer in stellar and planetary atmospheres. At high laser intensities all three components were found to saturate. The results were compared with the theoretical predictions of Mollow's steady-state theory. Theoretical fits for the high-intensity results were obtained when the collisional cross sections were taken to be considerably smaller than in our low-intensity measurements. We believe the discrepancy lies in the use of a steady-state theory for a transient experiment. Effects of radiative trapping and spatial averaging are also discussed.

I. INTRODUCTION

In two previous Letters^{1,2} we reported on the first observation of the spectral resolution of light scattered by an atomic vapor near a resonance line, and on the first experimental study of the spectral redistribution of light by collisions as a function of the detuning of the incident light. This paper is a summary and extension of these studies, giving details of the previous measurements and reporting later studies of saturation behavior. Basically, in all of our measurements we illuminate a cell containing Sr vapor (10^{-4} – 10^{-1} Torr) and Ar buffer gas (10–500 Torr) with a pulsed, tunable dye laser whose wavelength is near the 460.73-nm ($^1P_1^o - ^1S_0$) resonance line of Sr, and we analyze the spectrum of scattered light. In this Introduction we would like to put our measurements into perspective by pointing out their relation to other studies.

When a monochromatic light wave impinges on an atom near one of its resonance (absorption) lines, part of the light is scattered. In the absence of collisions and at low intensities, the spectrum of the scattered light is a single line centered on the incident wavelength, known as Rayleigh scattering. If the lower state is the ground state, the scattered light is monochromatic for a stationary atom³ and Doppler-shifted for a moving atom.⁴ If the lower state decays, the spectrum of the scattered light is broadened.^{5–8} If the atom that scatters the light collides with other atoms, the scattered light has a second component emitted near

the resonance frequency that is known as fluorescence. In a simple-minded description this component is due to the absorption of the incident light in the collision-broadened wing of the absorption line and its subsequent emission near line center. The theory of collisional redistribution has been developed from basic principles (the Kramers-Heisenberg dispersion formula, and collision dynamics) by Omont, Smith, and Cooper⁸ and Huber⁹ and is applicable in the central, impact region of the spectrum. No explicit theory for redistribution exists outside this region. The knowledge of the spectral and spatial redistribution of light scattered by atoms in the presence of collisions is of fundamental importance in the study of radiation transfer in stellar and planetary atmospheres.^{4,10} In fact we found it quite surprising that no direct measurements of the redistribution function had been made earlier.

Low-intensity absorption and emission measurements have been done for many years in atomic vapors broadened by a foreign gas. In fact, both the impact and the quasistatic theories of line broadening^{11–13} were developed to deal with these absorption¹⁴ and emission¹⁵ spectra. It is intuitively clear that the "excitation functions" (i.e., the dependence of the intensities of the various spectral components of scattered light on the incident frequency) are related to the absorption and emission spectra. In the impact region this relation can be shown explicitly from the general theory,^{8,9} and outside the impact region our experimental results suggest a similar connection.

When the incident light is strong, even for a noncolliding stationary atom and monochromatic incident field, three components appear. This was predicted first by Mollow¹⁶ and studied since theoretically by many^{6,7,17-22} who obtained essentially the same results. These components were observed in atomic beam experiments using very narrow cw dye lasers,²³⁻²⁵ and recent results agree²⁴ with the theory. In addition to the Rayleigh component mentioned above, there is a "three-photon" component that corresponds to absorption of two incident photons and the emission of another photon (a resonant Raman effect). Conservation of energy then requires the emission of one "fluorescence" photon on resonance. As the intensity is raised, all three components eventually saturate.

Scattering at high light intensity including the effects of collisions has been studied using several theoretical approaches. Mollow^{26,27} introduced phenomenological damping terms into his treatment of the collisionless atom scattering in a strong steady-state light field. This procedure is expected to give correct results if the "optical" cross section, which is related to the transition probability per incident photon, is independent of the (strong) incident flux. Another approach, to some extent complementary, was taken by Yakovlenko and co-workers,²⁸⁻³⁰ who studied the dynamics of atomic collisions in the presence of a classical (strong) incident field. They show that for weak fields the absorption reduces to the impact or quasistatic limits, implying a constant (in intensity) but frequency-dependent optical cross section. For high intensities they predict a change of the optical cross section. A similar study was done by Kroll and Watson³¹ and Lau.³²

There is yet another point of view of the scattering process that unifies and simplifies many calculations: that of the dressed atom and dressed molecule.^{22,33} The dressed atom state is the (adiabatic) eigenstate of the atom in a strong, single-mode external field—in the rotating-wave approximation. Light scattering can be viewed as spontaneous emission causing transitions among the various states.^{22,34} The absorption process during collisions can be viewed as a simple transition among these states: the ground state of the absorber before the collision and its excited state with one less photon in the field after the collision. A similar view, put forward originally by Yakovlenko *et al.*²⁸⁻³⁰ provides a unified picture of absorption, collision-induced absorption, and radiative ("optically induced", "switching") collisions.^{28-30,35,36}

A number of recent experiments indicate the importance of collisional redistribution of light.

Rousseau *et al.* have seen two different time dependences in their pulse-excited Raman spectra in iodine.³⁷⁻³⁹ Several authors have analyzed this experiment.^{34,40-42} Recently Liran⁴³ found that indeed the shifted (Raman) component follows the laser pulse in time and the fluorescence component decays with the lifetime of the upper state, as predicted.^{34,42} Collisional redistribution has been observed in resonance scattering from sodium in high-pressure helium,⁴⁴ from sodium in a dense high-temperature plasma,⁴⁵ and also from strontium vapor.⁴⁶ Collisional redistribution has been studied as an excitation mechanism in cesium-rare-gas mixtures.⁴⁷ In two-photon absorption, a "fast" off-resonance component and a "slow" on-resonance component were studied by Grischowsky.⁴⁸ The formation of molecules that occurs during collisional absorption of light has been utilized for spectroscopy by Gallagher¹⁵ and others⁴⁹ for many years.

In Sec. II we review the relevant theory as it exists. The experiment is described in Sec. III, and the results are analyzed in Sec. IV. Basically we studied the three emission components as a function of laser frequency, laser intensity and buffer gas pressure. There are also separate sections on our "auxiliary" experiments: studies of radiation trapping, measurements of absorption and emission spectra, and the measurement of the laser spatial profile. Section V presents a brief summary and discussion.

II. THEORY

A. Low laser intensities; collisional regime

Consider an atom and an incident monochromatic laser field, which, at the position of the atom, is

$$\vec{E}(t) = \hat{\epsilon}_L E \cos(\omega_L t), \quad (1)$$

where $\hat{\epsilon}_L$ is the polarization vector, ω_L is the incident frequency, and E is the electric field amplitude. The incident intensity of the laser in units of photons $\text{cm}^{-2} \text{sec}^{-1}$ is

$$I_L = cE^2/8\pi\hbar\omega_L. \quad (2)$$

The incident light frequency ω_L is taken to be near the atomic resonance frequency ω_0 , and the detuning Δ is defined by

$$\Delta = \omega_0 - \omega_L. \quad (3)$$

We now define the Rabi frequency on resonance:

$$\Omega = dE/\hbar, \quad (4)$$

where $d = e\langle 1 | \hat{\epsilon}_L \cdot \vec{r} | 2 \rangle$ is the electric dipole matrix element between the two relevant atomic states. Thus the laser intensity is proportional to the square of the Rabi frequency, $I_L \propto \Omega^2$. We make

the unrealistic assumption that both states are nondegenerate. When a 1S_0 state is coupled by linear polarized radiation to a $^1P_1^0$ state (as in our studies) this is a good approximation in the absence of collisions. In presence of collisions the picture has to be modified.⁵⁰ We also assume that the lower of these states $|1\rangle$ is the ground state, and the upper state $|2\rangle$ has a total damping rate γ (half width at half maximum) given by

$$\gamma = \gamma_N + \gamma_E + \gamma_I. \quad (5)$$

The unit of γ is rad/sec. The rate γ_N is due to the natural radiative decay of the excited state, while γ_E and γ_I result from elastic and inelastic collisions, respectively.

These damping processes are shown schematically in Fig. 1. The driving laser field is represented by the solid lines, spontaneous decay by the wavy line, and collisions by double lines. Elastic collisions are usually viewed as collisions which interrupt the phase of the emitted wave train. However, in the context of our work an elastic event can also be considered as a collision which transfers populations from the laser-excited virtual level to the real level. In this sense these events are actually "quasielastic" since the collisions must provide or absorb the energy difference $\hbar\Delta$. In contrast to this, inelastic collisions (quenching collisions) are those events which cause a net population transfer from the excited state to the ground state in a two-level system or to nearby levels in a multilevel system.

The theory has been worked out in detail for the impact region of the spectrum.^{8,9,40,41} The impact theory is valid only for pressures low enough that

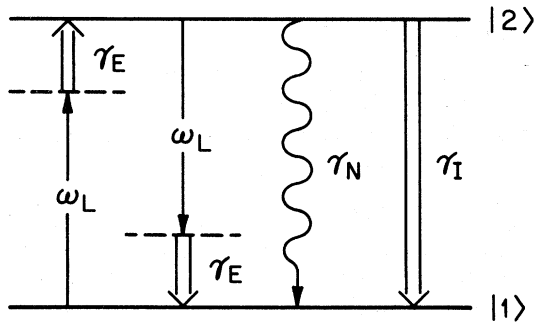


FIG. 1. Two-level atom with driving frequencies and damping rates. The straight arrows represent the laser field at frequency ω_L , while the wavy arrow represents radiation damping of the upper level at the spontaneous rate γ_N . The double arrows represent collisional damping: elastic collisions take the atom from the virtual level (dashed line) to the real level at a rate γ_E , while inelastic (quenching) collisions take the atom from level $|2\rangle$ to level $|1\rangle$ at a rate γ_I .

the duration of the collision is small compared to the time between collisions. In addition, it is applicable only for the frequency region close to line center. Mihalas⁴ has shown that the boundary frequency Δ_g , beyond which the impact approximation fails, is given (for a Van der Waals interaction) by

$$\Delta_g \approx 1.65 v^{3/2} N_p^{1/2} \gamma_E^{-1/2}, \quad (6)$$

where N_p is the density of the perturbers (in our case the argon atoms), γ_E is the half width at half maximum (HWHM) of the broadening due to elastic collisions, and v is the mean relative velocity of the emitting and perturbing atoms. The collisional linewidth is usually determined by experiment, or by specific theoretical calculations. For example, in Van der Waals broadening⁴

$$\gamma_E = N_p \sigma_E v, \quad (7)$$

where

$$\sigma_E = 4.04 (C_6/v)^{2/5}. \quad (8)$$

Here C_6 is the Van der Waals interaction constant.

Inside the impact region, for stationary atoms excited from their ground state by weak monochromatic light, the intensity distribution of the scattered light integrated over all angles and summed over polarizations, in steady state, in units of photons $\text{cm}^{-3} \text{sec}^{-1}$ is given by Huber's Eq. (4.8),⁹

$$I(\omega) d\omega = \left(\frac{\omega}{\omega_0}\right)^3 N \frac{(\gamma_N/2)\Omega^2 d\omega}{\Delta^2 + \gamma^2} \times \left[\delta(\omega - \omega_L) + \frac{\gamma_E}{\gamma_N + \gamma_I} \frac{\gamma/\pi}{(\omega_0 - \omega)^2 + \gamma^2} \right], \quad (9)$$

where N is the density of scatterers (in our case the strontium atoms), and the symbols are defined above.

The first term in this equation, which occurs at the incident frequency ω_L , is known as Rayleigh scattering and corresponds to the process shown in Fig. 2(b). The incident light is elastically scattered off a virtual state produced by the laser (shown as a broken line). Since the ground state has no natural width, the Rayleigh scattering has the same spectral profile as the excitation source.

The second term in Eq. (9) is the collision-induced fluorescence and corresponds to the process shown in Fig. 2(d). The laser-induced virtual state is collisionally transferred to the real excited state which then fluoresces with a Lorentzian profile centered at ω_0 and has a width equal to the sum of the natural and collisional widths. In the absence of collisions, the fluorescence vanishes and the scattered light maintains the profile of

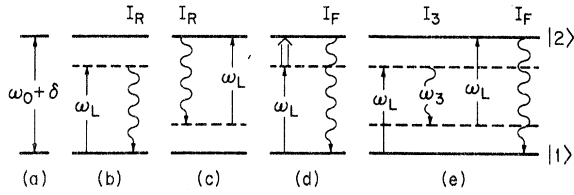


FIG. 2. (a) Two atomic levels separated by the unperturbed resonant frequency ω_0 plus the laser-induced Stark shift δ ; (b) Rayleigh scattering from the ground state at the laser frequency ω_L ; (c) Rayleigh scattering from the excited state; (d) collision-induced fluorescence at $\omega_0 + \delta$; (e) "three-photon" scattering at $\omega_3 = 2\omega_L - (\omega_0 + \delta)$ and consequent fluorescence at $\omega_0 + \delta$.

the incident light, even if the excitation source is narrower than and tuned inside the natural width of the resonance line.^{3,51}

In an atom whose upper and lower levels have spatial degeneracy, the angular distribution of the radiation and its polarization properties are complicated (cf. Omont *et al.*⁸). In our experiments the lower level is a 1S_0 state, and the upper one is 1P_1 ; therefore, the Rayleigh scattering has a classical dipole distribution, but the resonance fluorescence distribution depends on the details of the depolarization due to collisions.⁵⁰ In our experiment this is further complicated by the fact that our sample is optically thick on resonance; therefore the light that reaches our detector is multiply scattered. We have not studied these depolarization effects.

When the laser is tuned far off resonance, $|\Delta| \gg \gamma$, the two components can be resolved and the spectrally integrated intensities of the Rayleigh scattering I_R and collisionally induced fluorescence I_F are

$$I_R = N \left(\frac{\omega_L}{\omega_0} \right)^3 \frac{(\gamma_N/2)\Omega^2}{\Delta^2}, \quad (10)$$

$$I_F = N \left(\frac{\gamma_E}{\gamma_N + \gamma_I} \right) \frac{(\gamma_N/2)\Omega^2}{\Delta^2}. \quad (11)$$

Thus in the impact region, the integrated intensities of both the Rayleigh scattering and fluorescence behave as Δ^{-2} .

Note that Eq. (11) predicts that the integrated fluorescence signal I_F should be linear in laser intensity and also linear in the density of perturbers N_p ($\gamma_E \propto N_p$). However, the linearity holds only at low laser intensity and low pressure. In

Sec. IV we will see that at higher laser intensity or at high pressure, saturation occurs.

As $|\Delta|$ becomes larger than Δ_e , the impact approximation fails. Theories for the redistribution function outside the impact region have not been conveniently developed. (Huber⁹ has written down the integrals in terms of the time development operator, but they have not been solved.) However, since for $|\Delta| \gg \gamma$, collisions of the scattering atom do not change the Rayleigh intensity, we expect Eq. (10) to hold outside the impact region. Indeed far from line center, it goes over to the well-known Rayleigh scattering formula.⁵²

While collisions do not affect the Rayleigh intensity far from resonance, the fluorescence component depends heavily on the collision dynamics. Basically it depends on the ability of the collisions to supply (or absorb) the energy difference between the laser photon and the scattered photon. Indeed, far from resonance, the collision can no longer provide this energy difference efficiently and the cross section is expected to drop off.⁴² Even before the fall-off, non-Lorentzian shapes similar to those seen in emission and absorption experiments are expected. Accordingly, we will replace γ_E in Eq. (11) by the "empirical" elastic collision rate $\gamma_E(\Delta)$, which is a function of the detuning and will be indicative of a non-Lorentzian line shape. The cross section in Eq. (7) also becomes a function of detuning, denoted by $\sigma_E(\Delta)$.

Lisitsa and Yakovlenko³⁰ have shown the connection between $\sigma_E(\Delta)$ and the static theory of line broadening. It should be emphasized that the optical cross section $\sigma_E(\Delta)$ is not a cross section in the usual sense (although it does have dimensions of cm^2). The actual rate of production of excited atoms is described by the quantity $\sigma_E(\Delta)\Omega^2/\Delta^2$. Therefore it is proportional to the incident laser flux in dimensionless units.

B. High laser intensity; collisionless regime

We now discuss the distribution of scattered light when the laser intensity is allowed to become large, but when no collisions are present and Doppler broadening has been neglected. Recently there has been considerable theoretical interest in the spectrum of scattered light at high incident intensities.^{6,7,16-22} When $\Omega^2 + \Delta^2 \gg \gamma_N^2$, the intensity (photons $\text{cm}^{-3} \text{sec}^{-1}$) in steady state for monochromatic incident light is given by Mollow¹⁶ as

$$I(\omega) d\omega = \frac{N(\gamma_N/2)\Omega^2 d\omega}{\Delta^2 + \Omega^2/2} \left[\frac{\Delta^2 + \gamma_N^2}{\Delta^2 + \Omega^2/2} \delta(\omega - \omega_L) + \frac{\Omega^4/4}{(\Delta^2 + \Omega^2)(\Delta^2 + \Omega^2/2)} \left(\frac{s/\pi}{(\omega - \omega_L)^2 + s^2} \right) + \frac{\Omega^2/4}{(\Delta^2 + \Omega^2)} \left(\frac{\xi/\pi}{[\omega - \omega_L + (\Delta + \delta)]^2 + \xi^2} + \frac{\xi/\pi}{[\omega - \omega_L - (\Delta + \delta)]^2 + \xi^2} \right) \right], \quad (12)$$

where the widths of the Lorentzian emission profiles are given by

$$s = \gamma_N \left(\frac{\Omega^2 + 2\Delta^2}{\Omega^2 + \Delta^2} \right), \quad \xi = \gamma_N \left(\frac{\frac{3}{2}\Omega^2 + \Delta^2}{\Omega^2 + \Delta^2} \right), \quad (13)$$

and the other terms are defined in Sec. II A with the exception of δ which is the ac Stark shift given by

$$\delta = \Delta \{ [1 + (\Omega/\Delta)^2]^{1/2} - 1 \}. \quad (14)$$

Note that at low intensities the shift becomes

$$\delta = \frac{1}{2} \Omega^2 / \Delta \quad (\Omega \ll |\Delta|), \quad (15)$$

which is the well-known result derived from second-order perturbation theory.⁵³

There are four components in the emission spectrum given by Eq. (12). The first two terms are centered at the frequency of the incident laser. These terms are identified as the coherent and incoherent parts of the Rayleigh scattering, respectively, and are shown at ω_L in Fig. 3. The incoherent Rayleigh component is unimportant at low intensities but becomes dominant at high laser intensities. The third and fourth terms are centered at $\omega = \omega_L - (\Delta + \delta)$ and $\omega = \omega_L + (\Delta + \delta)$. These "side bands," which have recently been observed experimentally by a number of researchers,^{1, 23-25} are due to higher-order photon interactions. The process leading to these side bands is depicted in Fig. 2(e). With the laser tuned to $\omega_L \neq \omega_0$, two laser photons are absorbed, a photon is emitted and an excited state produced. This "three-photon"

component is given by the third term and is shown as the profile at ω_3 in Fig. 3. Since an excited state is produced for every photon generated at ω_3 , there will also be emission at $\omega_0 + \delta$ from the excited atom. This is the origin of the other side band which is shown as the *broken* profile at ω_0 in Fig. 3. Thus the two side bands have equal intensities. When the excitation laser is tuned to resonance, these two peaks occur as side bands located at $\omega_L + \Omega$ and $\omega_L - \Omega$. Therefore when the laser is tuned to resonance, one sees the Rayleigh emission at ω_L with two side bands each shifted by the Rabi frequency from the resonance. At this point it is useful to think of the side bands as resulting from the modulation of the resonance frequency ω_0 by the Rabi frequency Ω .²²

Having discussed the higher-order photon interactions, we can now understand the dependence of the two Rayleigh components on laser intensity. The coherent Rayleigh scattering, linear in laser intensity, is scattering off the ground state by a single laser photon. The incoherent Rayleigh scattering, cubic in laser intensity, indicates the following process: Two laser photons are absorbed to give an excited state as in Fig. 2(e) which Rayleigh scatters a third laser photon as in Fig. 2(c). As the excited state has a width, this gives rise to the width s of the incoherent Rayleigh scattering.^{22, 54}

When $\Omega^2 + \Delta^2 \gg \gamma_N^2$ the side bands can be resolved from the central Rayleigh scattering and Eq. (12) can be integrated over ω , giving the integrated Rayleigh intensity I_R (the sum of the coherent and incoherent components) and the integrated side bands I_3 and I_F , due to the "three-photon" scattering and the subsequent fluorescence, where

$$I_R = N \frac{(\gamma_N/2)\Omega^2}{\Delta^2 + \Omega^2} \quad (16)$$

and

$$I_3 = I_F = N \frac{(\gamma_N/8)\Omega^4}{(\Delta^2 + \Omega^2)(\Delta^2 + \Omega^2/2)}. \quad (17)$$

As before, the Rayleigh scattering can be viewed as emission from the laser-excited virtual level. At low intensities when the excited state population is small, we can associate a population $(N/2)[\Omega^2/(\Delta^2 + \Omega^2)]$ with this virtual level. If we let this "state" radiate at a rate γ_N , we obtain Eq. (16). An analogous argument can be made at higher laser intensities by including scattering off the excited state.

Equation (16) predicts that at high intensities the Rayleigh intensity I_R will saturate. This process can be viewed as an equalization of the population in the virtual and real states. It is a manifestation of the limitation on the spontaneous scatter-

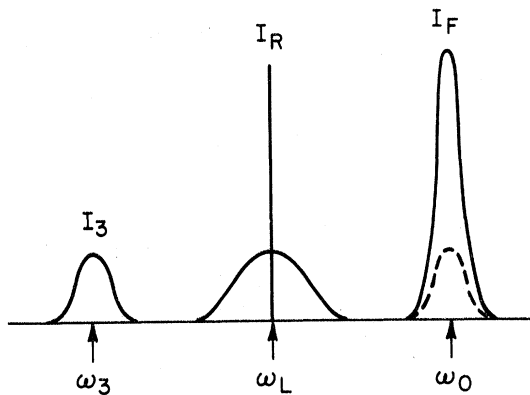


FIG. 3. Sketch of the emission spectrum of a two-level atom strongly driven near resonance by a monochromatic excitation source at frequency ω_L . In the presence of collisions, the spectrum consists of the four components shown by solid lines: coherent (narrow) and incoherent (broad) Rayleigh scattering at ω_L , "three-photon" emission at ω_3 and resonance fluorescence at ω_0 produced by both elastic collisions and the "three-photon" process. In the absence of collisions the fluorescence (broken line) has the same magnitude as the component at ω_3 .

ing intensity by the coupling constant to the vacuum, γ_N .

Equation (17) shows that at low intensities, the "three-photon" scattering and resulting fluorescence are proportional to the square of the laser intensity. At higher intensities, these components also saturate due to population equalization of the ground and excited states. Note that since the three-photon process corresponds to the generation of a photon and an excited atom, the process is a type of Raman scattering and therefore will have positive gain for a noninverted system. Stimulated emission of the component at ω_3 has been predicted⁵⁵⁻⁵⁹ and observed.⁶⁰⁻⁶³ Also, the emission of I_3 and I_F , the absorption of two laser photons and the return of the atoms to the ground state is a four-photon parametric process that has been discussed in the literature.⁶⁴

C. High laser intensity; collisional regime

In this section, we consider the effects of high laser intensities when collisions are also present. A number of papers have treated collisions through phenomenological relaxation terms, extending the treatment of the collisionless atom interacting with radiation.^{26,27,34,42,65} In all these treatments it was assumed that a strong incident electromagnetic field has no direct influence on the rate of colli-

sions, γ_E ; the main effect is to saturate the fraction of virtual levels and the population difference in the two-level system. Recently, collisions of atoms in the presence of the incident field were treated more accurately, and it has been pointed out that when the fields get strong they can directly influence the collision rates.²⁸⁻³² However the emission spectrum was not explicitly computed. Therefore we have chosen to treat the relaxation constant γ_E in Mollow's treatment^{26,27} as a free parameter.

Since we are primarily concerned with scattering at optical frequencies, the major collisional effect is due to elastic collisions. Inelastic collisions also have to be considered but are generally less frequent as they require large momentum transfers. At optical frequencies inelastic collisions that transfer the atom from the ground state to the excited state are usually negligible, since $\hbar\omega_0/kT$ is large.

We quote the results of Mollow's calculation,^{26,27} in which he added phenomenological relaxation terms to the equations of a strongly driven two-level system. The use of phenomenological relaxation terms gives rise to Lorentzian line shapes and is therefore only applicable in the impact regime of the spectrum [cf. Eq. (6)]. When $\Omega^2 + \Delta^2 \gg \gamma^2$, the scattered spectrum (in photons $\text{cm}^{-3} \text{sec}^{-1}$) in steady state is

$$I(\omega) d\omega = \frac{N(\gamma_N/2)\Omega^2 d\omega}{\Delta^2 + \eta\Omega^2} \left[\frac{\Delta^2 + \gamma^2}{\Delta^2 + \eta\Omega^2} \delta(\omega - \omega_L) + \frac{\Omega^2[(2\eta - 1)\Delta^2 + \eta^2\Omega^2]}{(\Delta^2 + \Omega^2)(\Delta^2 + \eta\Omega^2)} \left(\frac{s_1/\pi}{(\omega - \omega_L)^2 + s_1^2} \right) \right. \\ \left. + \frac{1}{2} \frac{(\Omega' - \Delta)[\eta(\Omega' - \Delta) + \Delta]}{(\Delta^2 + \Omega^2)} \left(\frac{\xi_1/\pi}{(\omega - \omega_L + \Omega')^2 + \xi_1^2} \right) \right. \\ \left. + \frac{1}{2} \frac{(\Omega' + \Delta)[\eta(\Omega' + \Delta) - \Delta]}{(\Delta^2 + \Omega^2)} \left(\frac{\xi_1/\pi}{(\omega - \omega_L - \Omega')^2 + \xi_1^2} \right) \right], \quad (18)$$

where the parameter η is defined as

$$\eta = (\gamma_N + \gamma_I + \gamma_E)/(2\gamma_N + 2\gamma_I). \quad (19)$$

The detuning parameter is defined as

$$\Omega' = \Delta + \delta, \quad (20)$$

and the widths of the profiles are

$$s_1 = (\gamma_N + \gamma_I) \left(\frac{2\eta\Omega^2 + 2\Delta^2}{\Omega^2 + \Delta^2} \right), \quad (21)$$

$$\xi_1 = (\gamma_N + \gamma_I) \left(\frac{(1 + \eta)\Omega^2 + 2\eta\Delta^2}{\Omega^2 + \Delta^2} \right).$$

The four terms in Eq. (18) are analogous to the terms given in Eq. (12) for the collisionless case. Therefore we will refer to these terms as coherent Rayleigh scattering, incoherent Rayleigh scattering, "three-photon" scattering, and fluorescence, respectively. One effect of the collisions is to increase the widths of the Lorentzian

profiles. However, the intensities of the various components are also affected. The largest change occurs in the fluorescence which can now occur both by the three-photon process and by direct collisional transfer from the laser excited virtual level. Thus it is always larger than the three-photon component, as shown in Fig. 3.

We can now see from Eq. (18) that the condition of "weak excitation" can be precisely stated as

$$\eta\Omega^2 \ll \Delta^2. \quad (22)$$

When the laser is "weak" and the collision rates are low, the spectrum given by Eq. (18) reduces to the low intensity limit given by Eq. (9). When $\Omega^2 + \Delta^2 \gg \gamma^2$, the components can be resolved and the integrated Rayleigh intensity I_R is again given by Eq. (16). While the collisions affect the coherent and incoherent Rayleigh intensities separately, the sum I_R is unaffected because Rayleigh scat-

tering can occur off ground or excited states; thus collisions do not affect the number of scattering centers. The integrated side bands I_3 and I_F are given by

$$I_3 = \frac{N(\gamma_N/4)\Omega^2(\Omega' - \Delta)[\eta(\Omega' - \Delta) + \Delta]}{(\Delta^2 + \Omega^2)(\Delta^2 + \eta\Omega^2)}, \quad (23)$$

$$I_F = \frac{N(\gamma_N/4)\Omega^2(\Omega' + \Delta)[\eta(\Omega' + \Delta) - \Delta]}{(\Delta^2 + \Omega^2)(\Delta^2 + \eta\Omega^2)}. \quad (24)$$

When η depends on the detuning, as will be the case outside the impact regime, the theory has not been worked out. We expect that the integrated intensities will be given by Eqs. (23) and (24), but that the line shape will not be Lorentzian. In fact, we expect that as long as the strong laser intensity has no direct influence on the collision rate, $\eta(\Delta)$ can be obtained from low-intensity measurements of $\sigma_E(\Delta)$.

It should be noted that a simple theory,³⁴ using dressed states gives all the results for integrated intensities correctly and also is valid in the transient regime.

III. EXPERIMENTAL APPARATUS

The strontium resonance line ($5s5p\ ^1P_1^o - 5s^2\ ^1S_0$) is located at 460.73 nm (21 698.482 cm^{-1}). The oscillator strength of this transition is $f = 1.94$ corresponding to a radiative lifetime of 4.68 nsec.⁶⁶ Since strontium is predominantly an even-even nucleus (93%), there is no hyperfine structure. Therefore, in the absence of collisions, this system will respond to a linearly polarized laser beam as a two-level system.

A nitrogen-laser-pumped dye laser was tuned near this 460.73-nm resonance line as shown in Fig. 4 and focused into an oven containing stron-

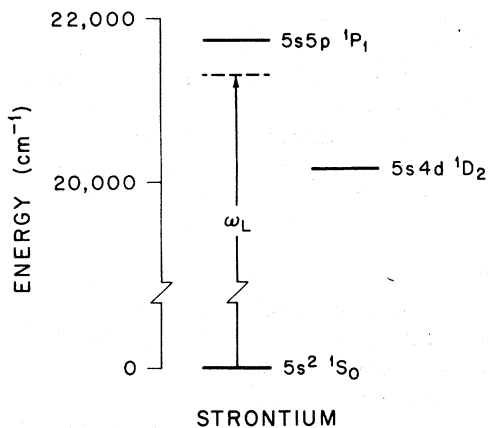


FIG. 4. Simplified energy levels for Sr. The laser, with frequency ω_L , is tuned near the $5s^2\ ^1S_0 - 5s5p\ ^1P_1$ resonance line located at 21 698.482 cm^{-1} (460.73 nm).

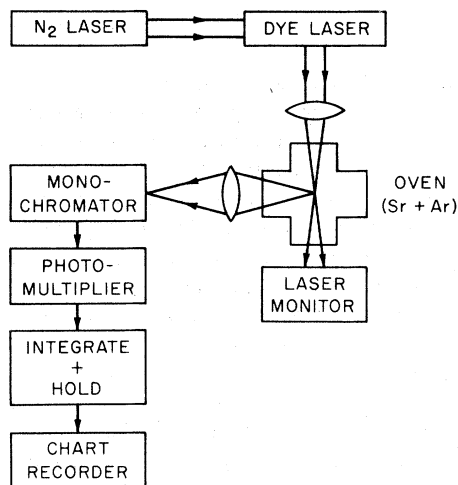


FIG. 5. Schematic diagram of experimental apparatus.

tium vapor and argon buffer gas. A schematic of the experimental apparatus is shown in Fig. 5. The oven was generally run with a buffer gas pressure of 10–500 Torr and in a temperature range of 400–500 °C. At 500 °C the vapor pressure of strontium is $\sim 8 \times 10^{-3}$ Torr and the Doppler width (half width at e^{-1} height) of the 460.73-nm resonance line is 2.8×10^{-2} cm^{-1} (5.9×10^{-4} nm). The side emission from the excited region in the oven was spectrally analyzed. Details of the apparatus are discussed below.

A. Dye laser

The dye laser was pumped by a modified version of an N_2 laser described by Woodward *et al.*⁵⁷ in the standard transverse pumping arrangement with a $\times 10$ beam expander and an Echelle grating (316 lines/mm). The N_2 laser output was focused into the dye cell with a simple quartz lens (18 cm focal length). The dye cell was a variation of a basic design by Drullinger⁶⁸ and consisted of a stainless-steel block fitted with a quartz entrance window and two 30' wedged side windows which were canted at 5° to prevent multiple reflections. All three windows were sealed to the stainless cell with Teflon O rings. The dye was flowed through the cell with a system containing parts made of stainless steel, Teflon, and polyethylene and including a Millipore filter. The output of the dye laser was almost totally linearly polarized with a linewidth of 1.4 cm^{-1} (0.03 nm) and a half-angle beam divergence of 1 mrad. The laser had a 5 nsec pulse length and an energy of ~ 0.2 mJ at the oven entrance. The dye laser beam was focused into the oven with a $\times 5$ beam contractor.

B. Oven

The vapor cell oven was made from 2-in.-diam stainless-steel tubing in the shape of a cross with 20-cm legs and with asbestos-insulated nichrome heater wire wound around the legs. Each leg of the cross was fitted with a window. Thermocouples and a temperature controller were used to maintain the temperature to within $\pm 2^\circ\text{C}$. The strontium was held in a stainless-steel boat with 5 mm holes in each end to allow passage of the laser and 3×10 mm slits in the sides to allow the side emission to be studied. Since we were looking at Rayleigh emission with the same frequency as the laser, spurious scatter had to be carefully avoided. To facilitate this, the windows through which the laser passed were set at an angle to avoid back reflections. To protect the windows in the oven, water cooling coils were attached to the stainless cross near the windows. In addition, a buffer gas of Ar of at least 10 Torr kept the windows from being coated with Sr.

C. Detection system

The side emission was studied with an $f/10$ detection system. By using a periscope the excitation region, which was approximately a cylinder of 110 μm diameter, was imaged parallel onto the slit of a 0.3-m McPherson model 218 monochromator using two camera lenses. By scanning one of the lenses in the detection optics, we measured the spatial profile of the Rayleigh scattering at low intensities. Using this profile, we estimated the peak power of the laser at the center of the excitation region to be 55 MW/cm². The resolution of the monochromator was 0.03 or 0.06 nm depending on the grating installed. The output of the RCA 7326, S-20 photomultiplier, which was placed at the exit of the monochromator, was fed into a gated (10 μsec) analog integrate-and-hold circuit and recorded on a chart recorder with a 1.5-sec time constant. The monochromator measured the wavelength to a resettable accuracy of 0.01 nm.

IV. EXPERIMENTAL STUDIES

When the dye laser was tuned near the $^1P_1^o - ^1S_0$ resonance transition at 460.73 nm, three components were observed in the side emission as predicted by the theoretical discussion of Sec. II. Figure 6 shows the spectral distribution of the side emission for two different laser intensities with the laser tuned to 460.56 nm ($\Delta = -8.0 \text{ cm}^{-1}$), the blue side of the resonance. The central component, which occurs at the excitation frequency ω_L , is the Rayleigh scattering. The width of this

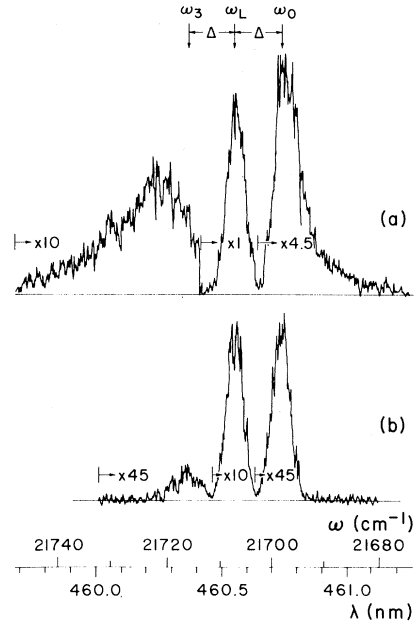


FIG. 6. Emission spectra for the laser tuned to the blue side of resonance ($\Delta = -8.0 \text{ cm}^{-1}$). (a) Full laser intensity, (b) laser attenuated by a factor of 50. The factors give the detection sensitivity. Observed are the Rayleigh scattering at ω_L , the resonance fluorescence at ω_0 and the "three-photon" scattering at ω_3 .

component is 0.07 nm which is determined primarily by the resolution of the monochromator.

The component near $\omega_3 = \omega_L - \Delta$ is due to three-photon scattering. Note that at high laser intensity it is considerably shifted due to the ac Stark effect. Since our laser is pulsed, this effect shows up both as a shift and a broadening as seen previously by others.^{69,70} The fluorescence component is located near the resonance frequency ω_0 . This component is a result of both three-photon scattering and collisional redistribution. At high laser intensity this component is also shifted and broadened. Since the lifetime of the excited state is comparable to the laser pulse length, only part of the fluorescence is emitted during the time the laser is on. Thus the shift and broadening of the fluorescence due to the ac Stark effect are not as large as those of the three-photon component, which is emitted only during the laser pulse.

We studied these emission components as a function of argon pressure, laser detuning, and laser intensity. All the data to be presented will be given as the integrated intensities of the resolved spectral components: I_R , I_F , and I_3 . These values were obtained by graphically integrating scans such as those in Fig. 6 and are thus limited in precision by noise in the apparatus. We estimate the precision of these measurements to be $\pm 20\%$.

A. Emission versus detuning at low laser intensities

We studied the effect of detuning on the integrated Rayleigh emission I_R and integrated fluorescence I_F at low laser intensities over a large range of Δ . The oven was run at a temperature of 530 °C and an argon buffer gas pressure of 50 Torr. At this temperature the number density of strontium was estimated to be $9.7 \times 10^{13} \text{ cm}^{-3}$ from vapor pressure data.⁷¹ In making the measurements, the linearity with laser intensity was checked for each point. This check eliminated the possibility of multiphoton and saturation effects and guaranteed that we were in the low intensity regime. In particular it guaranteed that the fluorescence was due only to collisional transfer from the virtual level and not to the higher-order three-photon process.

1. Rayleigh emission versus detuning

Since we were always in the region where $|\Delta| \gg \gamma$, we expected from Eq. (10) that the Rayleigh intensity should fall off as Δ^{-2} . The results are shown in Fig. 7 for detunings on both sides of resonance. The dashed curve shows the predicted Δ^{-2} dependence adjusted for the overall gain of the detection system. We see that for two decades of detuning, the integrated Rayleigh intensity goes as Δ^{-2} . Note that Δ was never large enough for the quadrupole allowed $^1S_0 \rightarrow ^1D_2$ transition (cf. Fig. 4) to affect the Rayleigh scattering. In Fig. 7 scattering from the surface of the oven (of the order of I_R at $\Delta = 200 \text{ cm}^{-1}$) was subtracted. We were not able to measure the Rayleigh scattering at $\Delta \approx +5 \text{ cm}^{-1}$ since the red absorption wing of the atoms surrounding the excitation region at-

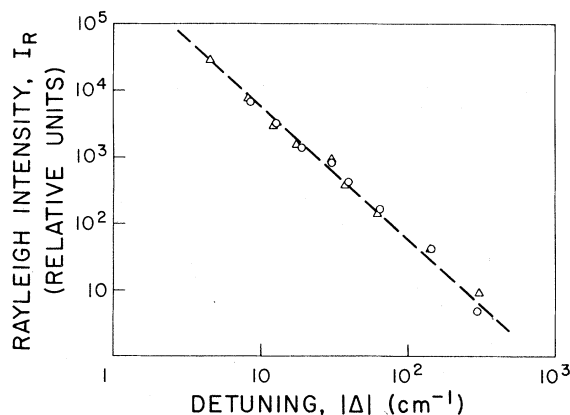


FIG. 7. Rayleigh scattering (spectrally integrated) versus detuning of the laser from resonance at low laser intensity. Detunings to the blue and red sides of resonance are shown by triangles and circles, respectively. The broken line shows the expected Δ^{-2} Lorentzian fall-off.

tenuated the Rayleigh intensity. The effect of ground-state atoms surrounding the excitation region and the resulting radiative trapping will be more fully discussed in the next section when we consider the fluorescence component.

2. Fluorescence versus detuning

In our experiment, the impact approximation is expected to be valid only for $|\Delta| < 4.6 \text{ cm}^{-1}$. This was determined using the measurements of Penkin and Shabanova⁷² and our Eq. (6). Thus we expect that for $|\Delta| > 4.6 \text{ cm}^{-1}$, the impact approximation will fail and the collision-induced fluorescence will no longer be Lorentzian. Experimentally we find that indeed the fluorescence is strongly frequency dependent and asymmetric. The composite spectral scans of Fig. 8 show that the fluorescence component, near ω_0 (slightly displaced by the ac Stark effect) is an order of magnitude larger when the laser is tuned to the red side of the resonance than when tuned to the blue.

Figure 9 shows experimental curves for the integrated intensity of collision-induced fluorescence as a function of Δ . The data at 5- cm^{-1} border the impact region. The units of I_F are relative to I_R of Fig. 7. The vertical error bars were determined by the scatter of several experimental readings for each point, while the horizontal bars simply show the 1.4 cm^{-1} uncertainty in frequency due to the laser linewidth. Also drawn is a broken curve for a Lorentzian fall-off corresponding to a constant γ_E in Eq. (11), where γ_E is taken from the pressure-broadening measurements.⁷² The broken

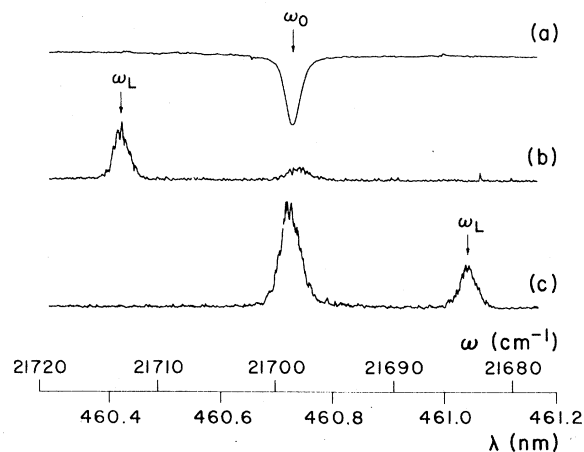


FIG. 8. Spectra showing asymmetry of fluorescence, at ω_0 , as a function of the laser frequency ω_L . (a) White light absorption profile showing location of resonance, (b) and (c) show the laser detuned from resonance by plus and minus 15 cm^{-1} , respectively. While the Rayleigh emission is symmetric with detuning, the collision-induced fluorescence is highly asymmetric.

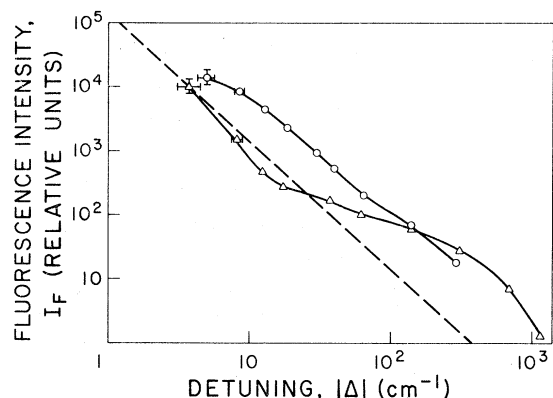


FIG. 9. Collision-induced fluorescence (spectrally integrated) as a function of detuning of the laser from resonance. Detunings to the blue and red sides of resonance are shown by triangles and circles, respectively. The broken line shows the Δ^{-2} dependence, valid in the impact region, extended to large detunings. Impact approximation is only valid for $|\Delta| < 4.6 \text{ cm}^{-1}$.

curve was corrected for self-absorption of the sample (see Sec. IV A 3 on radiative trapping).

It is seen from Fig. 9 that γ_E is strongly frequency dependent, as discussed in Sec. II A. In particular, when the laser is tuned to the red side of resonance, the fluorescence is initially much larger than when the laser is tuned to the blue. This "red wing" is very similar to the results found in absorption and emission experiments. This similarity is due to the fact that all these experiments effectively measure the collisional line shape of the transition. In particular, our experiment can be viewed as an absorption event followed by an emission event.

The origin of the red wing can be understood from very basic ideas involving potential curves. Figure 10 shows a schematic representation of the potential curves for the strontium-argon collision. Since the $\text{Sr}(^1P)$ level is more polarizable than the $\text{Sr}(^1S)$, the potential curve for the $\text{Sr}(^1P)\text{-Ar}(^1S)$ collision will be more attractive than the potential curve for the $\text{Sr}(^1S)\text{-Ar}(^1S)$ collision. When the laser is tuned to the red side of the resonance, the frequency of the laser will be equal to the difference potential at some internuclear separation and there will be a large overlap between the upper and lower state wave functions. Thus, according to the Franck-Condon principle, a transition will be induced. This side of resonance is referred to as the quasistatic wing.¹³ On the other hand, when the laser is tuned to the blue side of resonance, the overlap is less so that the collision-induced fluorescence is smaller. This side of resonance is referred to as the antistatic wing.¹³ When the laser is tuned far off resonance the repulsive parts of the curves will become important.

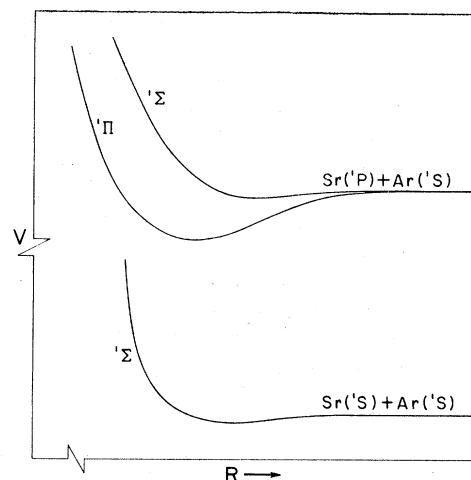


FIG. 10. Schematic drawing showing the general behavior of the potentials for a collision between the strontium (1P or 1S) atom and the ground-state argon atom.

For instance as seen from the schematic of Fig. 10, when the laser is tuned far off resonance to the blue, the $^1\Sigma$ upper curve and the $^1\Sigma$ lower curve run parallel so that the difference potential is constant and the transition probability increases. In our experiment this is probably the reason why the blue wing becomes more significant for large detunings.

In order to bring out the dependence on Δ more clearly, the quantity $\sigma_E(\Delta)$ is plotted versus Δ in Fig. 11. This was determined by the ratio of I_F/I_A

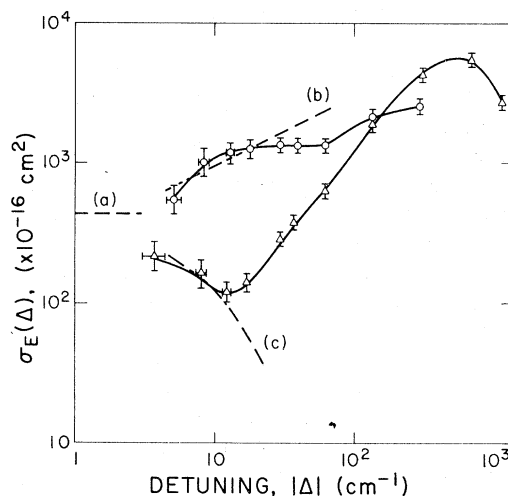


FIG. 11. Cross section σ_E for collision-induced fluorescence as a function of detuning at 530°C . Detunings to the blue and red sides of resonances are shown by triangles and circles, respectively. The dashed curves show the prediction of the theory of Szudy and Baylis (Ref. 13) using a Van der Waals interaction constant $C_6 = 9.8 \times 10^{-31} \text{ cm}^6 \text{ sec}^{-1}$: (a) the impact region, (b) the quasistatic region, and (c) the antistatic region.

I_R from Figs. 7 and 9. Account was also taken of the attenuation due to radiative trapping as discussed in the next section. The rate of collisional quenching was determined self-consistently from the measurements of Sec. IV B to be $\gamma_I = 0.29\gamma_N$.

We have compared our results with the predictions of the line-shape theory of Szudy and Baylis.¹³ Using their predictions for the line shape from a R^{-6} Van der Waals potential, we obtained the dashed curves for the (a) impact region, (b) quasi-static region, and (c) antistatic region when we used a value of $C_6 = 9.8 \times 10^{-31} \text{ cm}^6 \text{ sec}^{-1}$. As can be seen in Fig. 11 the value of σ_E in the impact region ($|\Delta| < 4.6 \text{ cm}^{-1}$) is then predicted to be $4.4 \times 10^{-14} \text{ cm}^2$ for 530°C . This is higher than that obtained at 530°C from the data of Penkin and Shabanova⁷² ($2.3 \times 10^{-14} \text{ cm}^2$) and also Farr and Hindmarsh⁷³ ($3.6 \times 10^{-14} \text{ cm}^2$). The differences are within the expected uncertainty.

Under our experimental conditions we found that the broadening was entirely due to Sr-Ar collisions and not Sr-Sr collisions. This was expected in the impact region from measurements of collisional widths for Sr-Sr collisions and Sr-Ar collisions. The values^{72,74} of these widths at 530°C and 50 Torr of argon are $\gamma_E(\text{Sr-Sr}) = 5.6 \times 10^7 \text{ rad sec}^{-1}$ and $\gamma_E(\text{Sr-Ar}) = 1.2 \times 10^9 \text{ rad sec}^{-1}$. This expectation was confirmed by repeating the experiment with the strontium density lowered by a factor of 8 and observing no change in the shape of the profiles in Fig. 9. This is consistent also with our data on fluorescence versus argon pressure at a detuning of 9.4 cm^{-1} (see Sec. IV B).

For large detunings, a question arose as to the mechanism responsible for populating the excited state. Since our laser had a spectral width of 0.03 nm , the possibility of excitation by the spectral wings⁷⁵⁻⁷⁹ needed to be considered. In addition, the spectral wings of the laser can produce a continuum of excited states between $\hbar\omega_L$ and $\hbar\omega_0$ which could be collisionally transferred to the excited state. When the laser is tuned very far from resonance, this "cumulative wing effect" could dominate the "normal" collision-induced fluorescence arising from the virtual state at $\hbar\omega_L$. Direct excitation by spectral components at the transition frequency was expected to be negligible because the oven had an optical depth of ~ 800 , thus absorbing all components within the absorption line before reaching the excitation region. To verify this expectation and to show also that the "cumulative wing effect" was negligible under our conditions, we placed a 0.03-nm bandpass monochromator in the laser beam to filter out any spectral wings. When the fluorescence versus detuning data of Fig. 9 were taken again with the filter in, no differences were seen. Thus the col-

lision-induced fluorescence could be considered to arise entirely from collisional transfer from the virtual level at $\hbar\omega_L$ to the excited state, where the location of the virtual level is known only to within the line width of the laser.

3. Radiative trapping

The small cylindrical region of Sr atoms that is excited by the laser is surrounded by unexcited Sr atoms. Most of our experiments were done at densities where this unexcited region is many absorption lengths deep (~ 800). The simplest way to estimate the number density of strontium atoms and therefore the optical depth is by measuring the equivalent width of the absorption line.⁸⁰ This measurement can also be checked with vapor-pressure curves. As a result of the radiative trapping, the fluorescence component of the scattered intensity was heavily attenuated. The loss of intensity comes from two separate sources: first, radiative trapping lengthens the lifetime of the excitation so that any quenching mechanism that is present becomes more effective; second, because of the diffusion of the radiation, the size of the radiative region increases, therefore that part of the emission that is collected on the slit of the monochromator decreases.

In order to verify that the trapping did not change the shape of the curves in Fig. 9, but only the overall gain, we checked the linearity of the fluorescence signal in laser intensity at every data point by inserting a neutral density filter into the laser beam and observing the appropriate linear drop in fluorescence signal. At *high* laser intensities and *small* detunings, the ac Stark shift by the laser can be large enough to shift the emission frequency outside the absorption equivalent width, reducing the amount of trapping and leading to an increase in fluorescence signals. The linearity check justified our using a higher laser intensity to produce signals at *large* detunings and then normalizing all the points in Fig. 9 to some fixed laser intensity. That the fluorescence was linear in laser intensity indicated that no significant Stark effects were occurring for these measurements.

It was mentioned in the previous section that the broken line in Fig. 9 was corrected for self-absorption of the sample. This was done by multiplying Eq. (11) by a constant attenuation factor determined as follows. By lowering the oven temperature to 400°C (strontium density $\approx 5 \times 10^{11} \text{ cm}^{-3}$), we substantially reduced the amount of trapping. At this low density, however, fluorescence could be observed only at small detunings. When the emission was observed at both plus and minus 5 cm^{-1} detuning, which borders the impact region, the fluorescence relative to the Rayleigh scatter-

ing was within a factor of 3 of that predicted by Eqs. (10) and (11), indicating an absence of trapping. Thus we used the ratio of the relative fluorescence signals with and without trapping as our attenuation factor.

4. Comparison of redistribution line shape with absorption and emission experiments

Absorption experiments measure the extinction coefficient which is the attenuation of a well-collimated monochromatic light beam at frequency ω_L . On the other hand, in emission experiments, the atoms are excited near line center by monochromatic light, and the fluorescence spectrum is measured off line center. Equation (9) shows that in the impact region of the spectrum the line shapes measured in absorption and emission should be the same as the profile determined by the scattering experiment described in this paper. Outside the impact region, the theory has not been explicitly developed. We have done two crude experiments to determine if any major differences exist between these various experiments in the quasistatic and antistatic region.

Figure 12(a) shows a scan of the absorption profile of the 460.73-nm resonance line of strontium. In order to see the spectral wings we operated at a temperature of 580 °C and 595 Torr of argon. The scan was obtained with a dc broadband light source passing through the oven and focused onto the monochromator slit. As in our redistribution experiments, we see a large red wing. Figure 12(b) shows a scan of the emission profile for the same temperature and pressure conditions when

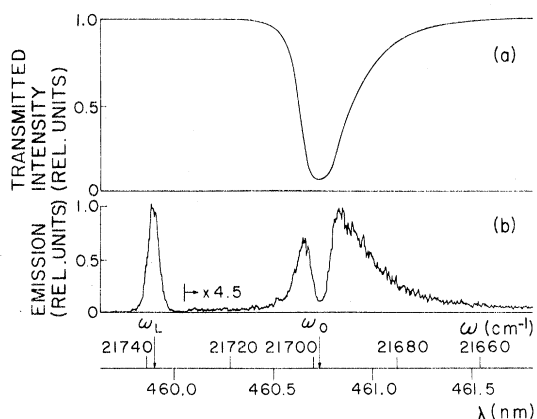


FIG. 12. (a) Scan of the absorption profile of the 460.73-nm line in strontium at 580 °C and 595-Torr argon. (b) Emission profile for the same experimental conditions with the laser tuned to 459.9 nm. Both profiles show a large red wing as do the redistribution results (Fig. 9). The factor gives the increase in detector sensitivity.

the laser was tuned to 459.9 nm. The Rayleigh emission is seen at the laser frequency as expected, and is as narrow as our resolution. As in both the redistribution experiment (Fig. 9) and the absorption experiment [Fig. 12(a)], the fluorescence line shape again has a strong red wing. Note that for this higher temperature and pressure the radiative trapping is evident from the dip in the fluorescence near ω_0 . We have determined the absorption profile $[-\log(I/I_0)]$ from Fig. 12(a) and also the emission profile from Fig. 12(b) and find that the shape of the profiles is the same as the redistribution profile shown in Fig. 9 to within a factor of 2.

B. Emission versus argon pressure

We have studied the fluorescence component as a function of argon buffer gas pressure with the laser tuned to 460.93 nm ($\Delta = 9.4 \text{ cm}^{-1}$). The study was done at a temperature of 400 °C so that effects of radiative trapping were minimal. Agreement with theory was obtained when the inelastic rate γ_I was taken to be linear in argon pressure. Experimental and theoretical curves showing the fluorescence versus Ar pressure at three different laser intensities are shown in Fig. 13.

The theoretical curves were computed from Eq. (24) with two adjustable parameters: γ_I and Ω^2 (laser intensity for curve a). The laser intensities for the lower curves were determined by the

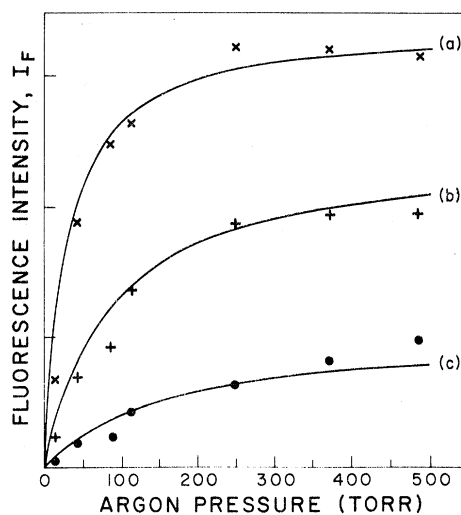


FIG. 13. Collision-induced fluorescence (spectrally integrated) as a function of argon buffer gas pressure for three different laser intensities. (a) Full laser intensity, (b) laser attenuated by 4.5, (c) laser attenuated by 20. The solid curves were computed from Eq. (24) with two common parameters: the quenching rate γ_I and the laser intensity for curve (a).

known attenuations of the neutral density filters used in the experiment. The value of γ_I determined by this fitting technique is $\gamma_I/\gamma_E = 0.007 \pm 0.002$. The value of Ω^2 was determined to be $\Omega^2/\Delta^2 = 0.1 \pm 0.03$ (0.5 MW/cm²). The radiative decay rate γ_N was taken⁶⁶ to be 1.07×10^8 rad sec⁻¹ and the elastic collision rate γ_E was determined self-consistently from the data in Fig. 11.

The general form of the curves for low laser intensity can be understood *qualitatively* by considering the rate scheme shown in Fig. 1. Following Eq. (17) it was pointed out that the "population" in the upper virtual level can be taken as $(N/2)(\Omega^2/\Delta^2)$. This "population" is then transferred to the upper state at a rate γ_E due to elastic collisions. Thus the transfer rate from the lower state to the upper state is $\gamma_T = (\gamma_E/2)(\Omega^2/\Delta^2)$. There is also a route for laser-induced collisional depopulation of the excited state. Thus we expect that the curves should be linear at low Ar pressure with the slopes increasing with increasing laser intensity and that each curve should saturate to some maximum fluorescence level, due to equalization of the excited and ground state populations. In the absence of quenching, all curves would saturate to the same level. This is because the transfer rate γ_T will eventually dominate the radiative decay rate γ_N . However, in the presence of quenching, there is a competition between the quenching rate γ_I and the transfer rate γ_T between levels so that each curve saturates to a different intensity as seen in Fig. 13. In fact, if the fluorescence is taken to be given by the decay rate γ_N times a steady-state population, we obtain $I_F = N\gamma_N[\gamma_T/(\gamma_I + \gamma_N)]$. It is interesting to note that Eq. (24), which was used to compute the curves in Fig. 11, reduces to this expression at low laser intensities.

C. Emission versus laser intensity

We studied the saturation of the three emission components at high laser intensities. The oven was run at 490 °C with an argon buffer gas pressure of 10 Torr. Thus, the number density of argon was $N(\text{Ar}) = 1.3 \times 10^{17}$ cm⁻³ and the number density of strontium was $N(\text{Sr}) = 2.5 \times 10^{13}$ cm⁻³.

In our initial comparisons with the theoretical predictions given by Eqs. (16), (23), and (24), we assumed the laser intensity was constant spatially. However, we found that at high degrees of saturation, there were deviations from the theory due to the nonlinear effects of the spatial wings of the laser. Therefore, we decided to average the theoretical predictions over the spatial profile of the laser. The method used for the spatial averaging is discussed below.

1. Spatial average

In the coordinate system shown in Fig. 14, the laser beam travels along the z direction (out of the page) and the detection system is along the x direction. For an emission profile $\epsilon(r)$, where r is the radial distance, the observed intensity profile is

$$I(y) = 2 \int_0^\infty \epsilon(r) dx = 2 \int_y^\infty \frac{r\epsilon(r) dr}{(r^2 - y^2)^{1/2}}. \quad (25)$$

By using the Abel inversion,⁸¹ $\epsilon(r)$ can be obtained:

$$\epsilon(r) = -\frac{1}{\pi} \int_r^\infty \frac{\{dI(y)/dy\} dy}{(y^2 - r^2)^{1/2}}. \quad (26)$$

To determine the laser profile $I_L(r)$ in the interaction region, we scanned the collection lens in the y direction while the monochromator observed the Rayleigh emission. The laser was run at low intensities so the Rayleigh emission was linear in laser intensity. Then by using Eq. (26) we found that the laser profile $I_L(r)$ (photons cm⁻² sec⁻¹) could be approximated by

$$I_L(r) = I_L \left(\frac{r_0^2}{r^2 + r_0^2} \right)^{3/2} \quad (27)$$

over the range of $r \leq 700$ μm . Outside this range our signal was in the noise. Here $I_L = I_L(r=0)$, and r_0 was found to be 110 μm . The spatial profile of the laser beam was then folded into Eqs. (16), (23), and (24) using Eq. (25). In this way, theoretical predictions for the three emission components as a function of laser intensity I_L were obtained, as presented in the following sections.

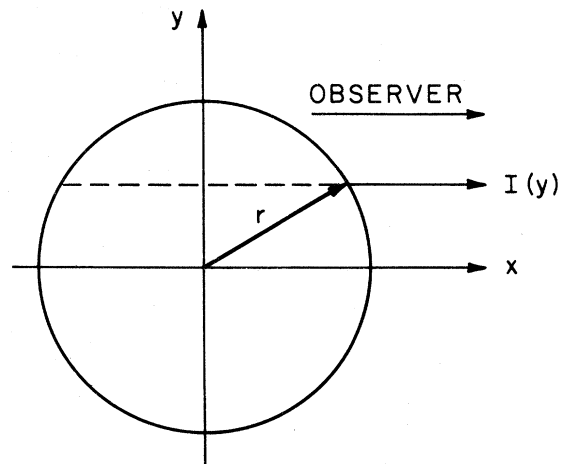


FIG. 14. Coordinate system for spatial averaging. The laser beam travels along the z axis (out of the page) and the detection system is in the x direction.

2. Rayleigh component

The dependence of the spectral integrated Rayleigh intensity on the incident laser intensity is given by Eq. (16). This equation shows that at low laser intensities, the dependence is linear in laser intensity. However, when $\Omega^2 \approx \Delta^2$, saturation begins to occur and the Rayleigh intensity falls below the linear dependence, eventually becoming constant.

We studied the saturation effect of the Rayleigh scattering at several detunings of the laser on both sides of resonance. The results are shown in Fig. 15 where it is seen that the saturation is less rapid when the laser is tuned far from resonance than when it is tuned near to resonance. The theoretical curves shown by the broken lines were obtained assuming a rectangular spatial profile for the laser and are therefore plots of Eq. (16) with two free parameters—the incident laser intensity and the overall detection sensitivity. All three curves use the same values for these parameters; only Δ was changed as measured experimentally. The fit was obtained with an incident laser intensity of 35 MW/cm². When a spatial average was taken as described in Sec. IV C 1, the theoretical curves shown by the solid lines were obtained. The fit was obtained with a laser intensity of 105 MW/cm² at the center of the excitation region. The deviation of the fit with and without spatial averaging is comparable to our experimen-

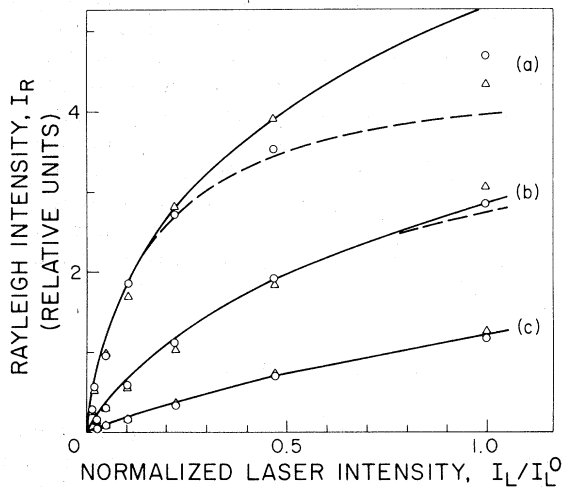


FIG. 15. Rayleigh scattering (spectrally integrated) versus laser intensity for several detunings. Detunings to the blue and red sides of resonance are shown by triangles and circles, respectively. (a) $\Delta = \pm 0.17$ nm, (b) $\Delta = \pm 0.36$ nm, (c) $\Delta = \pm 0.75$ nm. Near resonance, saturation is seen. The theoretical curves were obtained from Eq. (16) assuming a rectangular spatial profile (broken curves), and using the measured spatial profile given by Eq. (27) (solid curves). See Sec. IV C 2 for discussion.

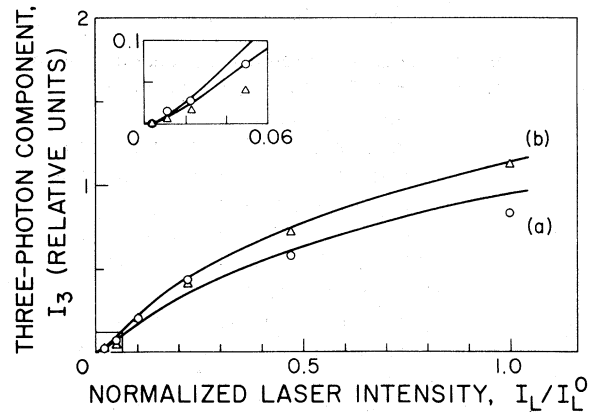


FIG. 16. Three-photon scattering (spectrally integrated) versus laser intensity for a detuning of 0.17 nm on the red side (a) and the blue side (b) of resonance. Solid curves are theoretical predictions using Eq. (23) with no free parameters. The insert shows the region at low intensity expanded by five. The intensity of the three-photon component is predicted to be quadratic in the region below a normalized laser intensity of 0.01. See Sec. IV C 3 for further discussion.

tal error. Note that for $|\Delta| = 0.75$ nm, spatial averaging does not change the theoretical curve.

3. Three-photon component

Theory predicts that at low intensities the three-photon component is quadratic in laser intensity but eventually saturates and levels off as does the Rayleigh intensity. As can be seen from Eq. (23), the integrated intensity I_3 of the three-photon component not only depends on the detuning and intensity of the laser, but also to a small degree on the collisional rates.

We have observed this three-photon component at the predicted position for both positive and negative values of the detuning Δ and for various laser intensities. In particular at $\Delta = \pm 0.17$ nm we have measured the intensity dependence of this component. The results are shown in Fig. 16. The vertical scale is the same relative scale used in plotting the Rayleigh intensity in Fig. 15. The curves shown in Fig. 16 are *zero* parameter predictions for the integrated intensity I_3 of the three-photon component using Eq. (23) and the values for the fixed parameters determined as follows. The overall sensitivity of the detection system, spatial average and incident laser intensity are the same as used to fit the Rayleigh saturation data in Fig. 15. Also γ_I was determined from our data presented in Sec. IV B. Finally, γ_E was determined from our low intensity data on the fluorescence (Fig. 11). We see that this zero parameter fit is within our 20% experimental accuracy.

4. Fluorescence component

We studied the laser intensity dependence of the spectrally integrated fluorescence at various detunings on both sides of resonance. Data at $\Delta = \pm 0.17$ nm are shown in Fig. 17. The relative units of the vertical scale of Fig. 17 are the same as in Fig. 15 for the Rayleigh intensity.

The solid curves in Fig. 17 are theoretical predictions using Eq. (24) with the spatial averaging procedure discussed in Sec. IV C 1. The fits were obtained using the elastic collision rate σ_E as a free variable. All other parameters were determined by previous data as for I_3 . The best fit to the data on the red side of resonance was obtained with $\sigma_E = 320 \times 10^{-16}$ cm². This is about a factor of 3 smaller than expected from our low-intensity measurements of the fluorescence shown in Fig. 11. On the blue side of resonance the best fit was for $\sigma_E = 18 \times 10^{-16}$ cm² which is a factor of 8 smaller than our low-intensity measurement.

The reason for this discrepancy probably lies in the fact that we have applied a steady-state theory to a pulsed experiment. Unlike the Rayleigh and three-photon components, which are only emitted during the laser pulse, the fluorescence

decays exponentially after the laser has turned off. As discussed in Sec. IV A 3 there is considerable radiation trapping due to the surrounding strontium atoms. At high laser intensities and small detunings, the ac Stark effect is large enough that the fluorescence emitted during the laser pulse is essentially untrapped. However, the fluorescence emitted after the laser pulse is heavily trapped, so that the total fluorescence is less than expected, leading to a smaller value of σ_E than expected. We are presently attempting to extend our analysis to a transient formulation using the theory of Courtens and Szöke.³⁴

We also have calculated the theoretical predictions for the fluorescence component without spatial averaging and using an incident laser power of 35 MW/cm² determined by the fit to the Rayleigh saturation data presented in Fig. 15. The resultant theoretical curves are shown in Fig. 17 by the broken lines. All other variables are the same as for the theory shown by the solid lines. Without spatial averaging, the theory predicts that the fluorescence at $\Delta = +0.17$ nm will saturate heavily. However, when we take the spatial average, the effect of extreme saturation is washed out by the spatial wings as seen by the solid curve. The reason that the effect of the wings is so much more important in the fluorescence than in the Rayleigh emission is that the slope of the fluorescence at low intensities is larger so that the wings are heavily weighted in the average.

We have also studied the fluorescence as a function of the intensity of the laser at larger detunings, where there is less saturation and the dependence is more linear. Good theoretical fits could be obtained using Eq. (24), but again all values of $\sigma_E(\Delta)$ determined from these fits were less than the values expected from the low intensity data shown in Fig. 11. As discussed above, we feel these differences are due to the steady-state assumption coupled with the effects of radiative trapping.

V. SUMMARY AND DISCUSSION

Our studies^{1,2} were the first ones that actually observed the collisional redistribution of scattered radiation. The knowledge of this function is important to the theory of radiative transport and line formation in stellar atmospheres. It has been calculated from first principles in the impact region, but no firm theory exists in the static region. Our experiments for low incident intensities can be summarized in terms of an empirical redistribution function that is similar to Eq. (9):

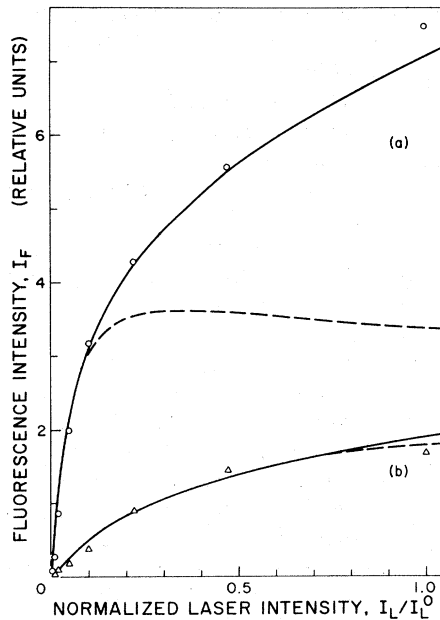


FIG. 17. Resonance fluorescence (spectrally integrated) versus laser intensity for a detuning of 0.17 nm on the red side (a) and the blue side (b) of resonance. Saturation on the red side is very pronounced. The theoretical curves were obtained from Eq. (24) assuming a rectangular profile (broken curve) and using the measured spatial profile given by Eq. (27) (solid curve). See Sec. IV C 4 for discussion.

$$I(\omega)d\omega = \left(\frac{\omega}{\omega_0}\right)^3 N \frac{(\gamma_N/2)\Omega^2 d\omega}{\Delta^2 + \gamma^2} \times \left(\delta(\omega - \omega_L) + \frac{\gamma_E(\Delta)}{\gamma_N + \gamma_I} f(\omega)\right). \quad (28)$$

where $\gamma_E(\Delta)$ can be obtained from Fig. 11. Here $f(\omega)$ is the emission line shape, normalized to $\int f(\omega) d\omega = 1$. We actually measured only pieces of this formula, i.e., $I_F \propto \gamma_E(\Delta)/\Delta^2$, $I_R \propto 1/\Delta^2$, and in a separate experiment $f(\omega)$, where we also found $f(\Delta) \propto \gamma_E(\Delta)/\Delta^2$ within our experimental range and error. We have also shown that experiments with variable perturber density can establish the inelastic collision rate γ_I , though we have done no experiments to determine the actual cause of quenching.

Radiation trapping, one of the major obstacles in our experiments, is an interesting subject by itself. We conducted enough experiments to convince ourselves that we can account for the influence of trapping consistently. It is interesting to note that experiments similar to ours can be conducted to study details of the space-time behavior of radiative trapping.⁸² By measuring the space-, time-, and spectrally-resolved scattered light after a small cylindrical region is excited by a pulsed laser, the most fundamental quantity in radiative transfer, the Green's function, can be measured experimentally.

The high-field behavior of the Rayleigh and three-photon scattering has been studied and agreement was obtained with Mollow's steady-state theory. While the integrated Rayleigh component

was found to be "collisionless," the third component was found to have a weak collisional dependence. The fluorescence component was also found to fit the steady-state theory quite well, but the cross section for the elastic collision was smaller than that predicted by our low intensity measurements. We feel that this discrepancy is due in part to the transient nature of the laser excitation because (a) there is not enough time for collisional equilibration, and (b) during the strong laser pulse the fluorescence is ac Stark shifted and therefore escapes, but after the pulse is over the rest of the fluorescence is trapped and partly lost to the detection system. It is interesting to note that according to recent studies³⁰⁻³² it is expected that the elastic collision rate should have some intensity dependence. We continue our studies in this direction.

Note added in proof. Recently Nienhuis and Schuller (private communication) have extended the theory of collisional redistribution into the far wing where the impact limit is invalid. They find that their predictions are in qualitative agreement with our observations of the asymmetry in the collisional redistribution.

ACKNOWLEDGMENTS

The authors wish to thank B. R. Mollow for making available his results prior to their publication, and also A. Gallagher for several very useful discussions on line broadening. In addition the authors acknowledge the helpful comments and suggestions of J. Cooper, W. C. Lineberger, and S. J. Smith.

*Research supported by the Office of Naval Research under Contract No. N00014-76-C-0611 and by the National Science Foundation under Grant No. MPS72-05169.

†Present address: Lawrence Livermore Laboratory, University of California, Livermore, California, 94550.

‡Department of Chemistry, University of Colorado, Boulder, Colorado 80309.

¹J. L. Carlsten and A. Szöke, Phys. Rev. Lett. **36**, 667 (1976).

²J. L. Carlsten and A. Szöke, J. Phys. B **9**, L231 (1976).

³W. Heitler, *The Quantum Theory of Radiation* (Clarendon, Oxford, 1957), 3rd ed.

⁴D. Mihalas, *Stellar Atmospheres* (Freeman, San Francisco, 1970).

⁵N. M. Kroll, in *Quantum Optics and Electronics, Les Houches Lectures 1964*, edited by C. DeWitt, A. Blaudin, and C. Cohen-Tannoudji (Gordon and Breach, New York, 1965).

⁶A. P. Kazantsev, Zh. Eksp. Teor. Fiz. **66**, 1229 (1974) [Sov. Phys.-JETP **39**, 601 (1974)].

⁷B. R. Mollow, Phys. Rev. A **13**, 758 (1976).

⁸A. Omont, E. W. Smith, and J. Cooper, Astrophys. J. **175**, 185 (1972); **182**, 283 (1973).

⁹D. L. Huber, Phys. Rev. **178**, 93 (1969).

¹⁰See, for example, J. L. Kohl and W. H. Parkinson, Astrophys. J. **205**, 599 (1976); T. R. Ayres and J. L. Linsky, Astrophys. J. **205**, 874 (1976).

¹¹For extensive review, see e.g., A. Ben-Reuven, Adv. Chem. Phys. **33**, 235 (1975); F. Schuller and W. Behmenburg, Phys. Rev. **12**, 273 (1974).

¹²For reviews see, e.g., J. Cooper, Comments on the theory of satellite bands, JILA Report No. 111, Univ. of Colorado, Boulder, Colo. 80309 (1973); also Refs. 10 and 70.

¹³J. Szudy and W. E. Baylis, J. Quant. Spectrosc. Radiat. Transfer **15**, 641 (1975).

¹⁴C. L. Chen and A. V. Phelps, Phys. Rev. A **7**, 470 (1973).

¹⁵A. Gallagher, in *Atomic Physics*, Vol. 4, edited by G. zu Putlitz, E. W. Weber, and A. Winnacher (Plenum, New York, 1975).

¹⁶B. R. Mollow, Phys. Rev. A **188**, 1969 (1969).

¹⁷S. S. Hassan and R. K. Bullough, J. Phys. B **8**, L147 (1975).

¹⁸H. T. Carmichael and D. F. Walls, J. Phys. B **9**, 1199 (1976).

¹⁹M. E. Smithers and H. S. Freedhoff, J. Phys. B **8**, 2911

- (1975).
- ²⁰B. R. Mollow, Phys. Rev. A 12, 1919 (1975).
- ²¹H. J. Kimble and L. Mandel, Phys. Rev. A 13, 2123 (1976).
- ²²C. Cohen-Tannoudji, in *Lecture Notes in Physics 43, Laser Spectroscopy*, Proceedings of the Second International Conference, Megeve, 1975, edited by S. Haroche, J. C. Pebay-Peyoula, T. W. Hänsch, and S. E. Harris (Springer, Berlin, 1975).
- ²³F. Schuda, C. R. Stroud, Jr., and M. Hercher, J. Phys. B 7, L198 (1974).
- ²⁴F. Y. Wu, R. E. Grove, and S. Ezekiel, Phys. Rev. Lett. 35, 1426 (1975).
- ²⁵W. Hartig, W. Rasmussen, R. Schieder, and H. Walther, Z. Phys. A278, 205 (1976).
- ²⁶B. R. Mollow, Phys. Rev. A 2, 76 (1970).
- ²⁷B. R. Mollow, preceding paper, Phys. Rev. A 15, 1023 (1977).
- ²⁸L. I. Gudzenko and S. I. Yakovlenko, Zh. Eksp. Teor. Fiz. 62, 1686 (1972) [Sov. Phys.-JETP 35, 877 (1972)].
- ²⁹V. S. Lisitsa and S. I. Yakovlenko, Zh. Eksp. Teor. Fiz. 66, 759 (1974) [Sov. Phys.-JETP 39, 759 (1974)].
- ³⁰V. S. Lisitsa and S. I. Yakovlenko, Zh. Eksp. Teor. Fiz. 68, 479 (1975) [Sov. Phys.-JETP 41, 233 (1975)].
- ³¹N. M. Kroll and K. M. Watson, Phys. Rev. A 13, 1018 (1976).
- ³²A. M. F. Lau, Phys. Rev. A 13, 139 (1976); 14, 279 (1976).
- ³³See, e.g., review by C. Cohen-Tannoudji, in *Cargèse Lectures in Physics*, Vol. 2 (Gordon and Breach, New York, 1968).
- ³⁴E. Courtens and A. Szöke, Phys. Rev. A (to be published).
- ³⁵S. E. Harris and D. B. Lidow, Phys. Rev. Lett. 33, 674 (1974).
- ³⁶D. B. Lidow, R. W. Falcone, J. F. Young, and S. E. Harris, Phys. Rev. Lett. 36, 462 (1974).
- ³⁷P. F. Williams, D. L. Rousseau, and S. H. Dworkin, Phys. Rev. Lett. 32, 196 (1974).
- ³⁸D. L. Rousseau, A. D. Patterson, and P. F. Williams, Phys. Rev. Lett. 34, 1306 (1975). See also a critique by P. A. Hackett, Phys. Rev. Lett. 36, 1403 (1976), and the authors' reply, Phys. Rev. Lett. 37, 1441 (1976).
- ³⁹D. L. Rousseau and P. F. Williams, J. Chem. Phys. 64, 3519 (1976).
- ⁴⁰S. Mukamel, A. Ben-Reuven, and J. Jortner, Phys. Rev. A 12, 947 (1975).
- ⁴¹S. Mukamel, A. Ben-Reuven, and J. Jortner, Chem. Phys. Lett. 38, 394 (1976).
- ⁴²A. Szöke and E. Courtens, Phys. Rev. Lett. 34, 1053 (1975).
- ⁴³Y. Liran, private communication, and unpublished.
- ⁴⁴R. D. Driver and J. L. Snider, Center for Astrophysics Preprint No. 551 (unpublished).
- ⁴⁵L. Vriens and M. Adriaansz, Appl. Phys. 11, 253 (1976).
- ⁴⁶K. Sakurai, A. Adams, M. Lambropoulos, and H. P. Broida, Bull. Am. Phys. Soc. 21, 1245 (1976).
- ⁴⁷R. T. M. Su, J. W. Bevan, and R. F. Curl, Jr. (unpublished).
- ⁴⁸D. Grischkowsky, Phys. Rev. A 14, 802 (1976).
- ⁴⁹R. E. Drullinger, M. M. Hessel, and E. W. Smith, NBS Monograph 143 (1975), and unpublished.
- ⁵⁰R. J. Ballagh and J. Cooper, Astrophys. J. (to be published).
- ⁵¹H. M. Gibbs and T. N. C. Venkatesan, IEEE J. Quantum Electron. 11, 91D (1975).
- ⁵²J. D. Jackson, *Classical Electrodynamics* (Wiley, New York, 1967), p. 603.
- ⁵³A. M. Bonch-Bruevich and V. A. Khodovoi, Usp. Fiz. Nauk. 93, 71 (1967) [Sov. Phys. Usp. 10, 637 (1968)].
- ⁵⁴This is an appealing, but *not* an accurate description of the process. In particular, the coherent component completely disappears when the incident field is strongly saturating.
- ⁵⁵S. A. Rautian and I. I. Sobel'man, Zh. Eksp. Teor. Fiz. 41, 456 (1961) [Sov. Phys.-JETP 14, 328 (1962)].
- ⁵⁶A. Javan, Phys. Rev. 107, 1579 (1957).
- ⁵⁷P. P. Sorokin, N. S. Shiren, J. R. Lankard, E. C. Hammond, and T. G. Kazyaka, Appl. Phys. Lett. 10, 44 (1967).
- ⁵⁸B. R. Mollow, Phys. Rev. A 5, 2217 (1974).
- ⁵⁹S. L. McCall, Phys. Rev. A 9, 1515 (1974).
- ⁶⁰N. N. Badalyan, V. A. Iradyan, and M. E. Movsesyan, Zh. Eksp. Teor. Fiz. Pis. Red. 8, 518 (1968) [JETP Lett. 8, 316 (1968)].
- ⁶¹V. M. Arutyunian, T. A. Papazyan, Yu. S. Chilingaryan, A. V. Karmenyan, and S. M. Sarkisyan, Zh. Eksp. Teor. Fiz. 66, 509 (1974) [Sov. Phys.-JETP 39, 243 (1974)].
- ⁶²D. B. Aleksandrov, A. M. Bonch-Bruevich, V. A. Khodovoi, and N. A. Chigir, Zh. Eksp. Teor. Fiz. Pis. Red. [JETP Lett. 18, 58 (1973)].
- ⁶³A. M. Bonch-Bruevich, V. A. Khodovoi and N. A. Chigir, Zh. Eksp. Teor. Fiz. 67, 2069 (1974) [Sov. Phys.-JETP 40, 1027 (1975)].
- ⁶⁴See, e.g., Y. R. Shen, Rev. Mod. Phys. 48, 1 (1976) for a recent review and extensive list of references.
- ⁶⁵T. J. McIlrath and J. L. Carlsten, Phys. Rev. A 6, 1091 (1972).
- ⁶⁶F. M. Kelly, T. K. Koh, and M. S. Mathur, Can. J. Phys. 52, 795 (1974).
- ⁶⁷B. W. Woodward, V. J. Ehlers, and W. C. Linberger, Rev. Sci. Instrum. 44, 882 (1973).
- ⁶⁸R. E. Drullinger (private communication).
- ⁶⁹P. F. Liao and J. E. Bjorkholm, Phys. Rev. Lett. 34, 1 (1975); Opt. Commun. 16, 392 (1976), and references therein.
- ⁷⁰D. Prosnitz, D. W. Wildman, and E. V. George, Phys. Rev. A 13, 891 (1976).
- ⁷¹R. E. Honig and D. A. Kramer, RCA Rev. 285 (1969).
- ⁷²N. P. Penkin and L. N. Shabanova, Opt. Spectrosc. 25, 446 (1968).
- ⁷³J. M. Farr and W. R. Hindmarsh, J. Phys. B 4, 568 (1971).
- ⁷⁴N. P. Penkin and L. N. Shabanova, Opt. Spectrosc. 26, 191 (1969).
- ⁷⁵S. Mukamel and J. Jortner, J. Chem. Phys. 62, 3609 (1974).
- ⁷⁶J. M. Friedman and R. M. Hochstrasser, Chem. Phys. 6, 155 (1974).
- ⁷⁷J. O. Berg, C. A. Langhoff, and A. W. Robinson, Chem. Phys. Lett. 29, 305 (1974).
- ⁷⁸H. Metiu, J. Ross and A. Nitzan, J. Chem. Phys. 63, 1289 (1975).
- ⁷⁹P. A. Hackett and R. A. Black, Chem. Phys. Lett. 37, 339 (1976).
- ⁸⁰J. L. Carlsten, J. Phys. B 7, 1620 (1974).
- ⁸¹R. Courant and D. Hilbert, *Methods of Mathematical Physics* (Interscience, New York, 1953), Vol. I, Chap. III.
- ⁸²A. V. Phelps (private communication).